A Singly-Fed Dual-Band Microstrip Antenna for Microwave and Millimeter-wave Applications in 5G Wireless Communication

Yu Qing Guo, Yong Mei Pan, *Senior Member*, *IEEE*, Shao Yong Zheng, *Senior Member*, *IEEE*, Kai Lu

***Abstract*— The coexistence of microwave (MW) and millimeter wave (MMW) technologies is considered as the development tendency of the future 5G wireless communication system. In this paper, a single-port, single-layer, dual-band antenna with large frequency ratio is proposed to support the MW and MMW applications. This antenna mainly consists of a stub-loaded microstrip line in the center, two slot-loaded rectangular patches on the lateral sides, and two thin microstrip lines in-between which connect the former two. The stub-loaded microstrip line works as a series-fed MMW linear array at 26 GHz, and simultaneously it serves as the feed line for the MW patches operating at 4.85 GHz. The connection lines are elaborately designed to isolate the MW patches from the MMW signal, guaranteeing the radiation performance of the antenna at the two bands without requiring complicated filter. For verification, a prototype is fabricated and measured. The measured results show that the antenna has an impedance bandwidth of 3.1% and a peak gain of 8.93 dBi at the 4.85-GHz MW band, while an impedance bandwidth of 19% and a peak gain of 13.57 dBi at the 26-GHz MMW band.**

***Index Terms*—Dual-band antenna, millimeter-wave antenna, microstrip antenna, large frequency ratio, 5G wireless communication.**

I. Introduction

At present, the microwave (MW) technology has already been successfully utilized to realize the 5th generation (5G) mobile networks [1]. Meanwhile, due to the advantages of millimeter wave (MMW) communication such as extremely high data rate, large transmission capacity, and good security, the MMW spectrum is widely considered to be a preferable choice for the future 5G wireless communication system [2]−[4]. However, the propagation of electromagnetic waves suffers from high pass loss and short transmission distance in MMW band [5], [6]. Therefore, there is every possibility that the MW and MMW technologies will coexist in the final stage of 5G, and they two are expected to complement each other [7],[8]. On the other hand, cellular mobile communication has great potential in the application of the Internet of Vehicles (IoV) due to the advantages of wide coverage, large capacity, and high security [9]. As a competitive IoV technology, the cellular Vehicle-to-everything (C-V2X) technology over the Uu interface supports Vehicle-to-Network (V2N) and Vehicle-to-Cloud (V2C) communications [10], and it operates at the spectrums of cellular mobile communication. Therefore, to make full use of the resources of cellular mobile communication, the future C-V2X communication based on cellular network may also concurrently work at both MW and MMW bands. As a result, the investigations of dual-band wireless devices including antennas which can work simultaneously in MW band and MMW band have great significance.

The dual-band antennas can be designed using two or multiple resonant modes of a certain radiator [11]−[17]. These antennas generally have a relatively simple structure and a single feed port [11]−[13], [16]. Nevertheless, the two operating bands of such dual-mode dual-band antennas are often both located in MW band [11]−[15] or MMW band [16], [17], and the frequency ratio is limited to less than 3. To obtain a dual-band antenna with large frequency ratio, one simple way is to directly combine two antennas working at different bands [18]–[20]. For example, a MW monopole antenna and a MMW microstrip grid array were placed side by side on a single-layer substrate in [18]. This arrangement makes the antenna design of different bands independent and flexible, imposing few restrictions on the frequency ratio. However, since the two MW and MMW antennas were just simply put together, the entire structure was not compact.

Recently, the shared-aperture dual-band antennas with large frequency ratios have attracted increasingly attention [21]–[24]. To share the aperture, a MMW dielectric resonance antenna (DRA) was nested into a MW slot antenna in [21], and in [22] a MW patch antenna was stacked vertically on the top of a MMW reflector array. The aperture-sharing concept has also been further extended to the structure-sharing scheme to design more compact MW and MMW dual-band antennas [25]−[33]. A leaky-wave antenna based on a dual-mode composite microstrip line was proposed for MW and MMW applications in [25]. On one hand, the quasi-TEM mode of the composite microstrip line was used to excite the MW patch array. On the other hand, the TE_{10}-like mode of the microstrip line was used to feed the MMW slot array. In [26], the short-circuited end of the Wi-Fi band PIFA antenna also functioned as the feeding network of the Wi-Gig band leak-wave antenna. The MW and MMW antennas even shared the same radiator in [27] and [28], by using the resonances of its different parts. Due to the aperture or structure sharing of the MW and MMW elements, the antenna size and weight can be reduced effectively. However, it is notable that all the above designs have two or

Manuscript received September 20, 2020; revised February 3, 2021; accepted March 23, 2021. This work was supported in part by the National Natural Science Foundation of China under Grant 61922031 and 61871187, and in part by the Guangdong Provincial Key Laboratory of Short Range Wireless Detection and Communication. (*Corresponding Author: Yong Mei Pan*)

Y. Q. Guo and Y. M. Pan are with the School of Electronic and Information Engineering, South China University of Technology, Guangzhou 510641, China. S. Y. Zheng and K. Lu are with the School of Information Science and Technology, Sun Yat-sen University, Guangzhou 510006, China (e-mail: eeympan@scut.edu.cn)

This article has been accepted for publication in a future issue of this journal, but has not been fully edited. Content may change prior to final publication. Citation information: DOI 10.1109/TVT.2021.3070807, IEEE Transactions on Vehicular Technology

multiple feed ports, and each port is separately used for each radiating element operating at different bands [21]−[33]. That is to say, the lower-band and the upper-band signals are transmitted from different ports and through different paths to the corresponding elements. Obviously, this is a direct way to reduce the mutual interference between MW band and MMW band, but not elaborate since two sets of feeding networks are required, which make the front end of antenna complicated.

Due to the large dimension difference between the MW and the MMW elements, it is a challenge to design a single-port dual-band antenna with large frequency ratio, and thus far, little work has been reported [34]−[36]. In [34], a singly-fed dual-band antenna operating in the WiFi and WiGig bands was realized, on a single-layer substrate. The WiFi band radiation was based on a printed monopole, while the WiGig band radiation was based on a higher-order mode patch. The two elements were placed back-to-back, and there was no shared structure. In addition, an extra compact microstrip resonance cell (CMRC) low-pass filter had to be used to isolate the WiFi monopole from the WiGig microstrip patch, which introduced unavoidable insertion loss and extra circuit size. The aperture coupling mechanism was skillfully used in [35] to block the MMW signal from feeding to the MW antenna element and simultaneously route it into the MMW element, realizing a single-port dual-band antenna with a frequency ratio of ~5. Nevertheless, the proposed method is only applicable to the slot coupling feed structure. Moreover, owing to the coupling structure, a two-layer configuration was resulted. A structure sharing, single-layer, dual-band microstrip grid array antenna was realized in [36]. This array utilized a single port to excite two modes operating in the MW and MMW bands respectively. Unfortunately, it required a differential feeding network and two large parasitic patches to improve the impedance matching, which complicated the design and enlarged the footprint.

In this paper, a single-port, single-layer, structure-sharing, dual-band antenna with large frequency ratio that can simultaneously cover the MW and MMW bands is investigated. This antenna utilizes a stub-loaded microstrip linear array to cover the 26-GHz 5G MMW band, while two slot-loaded rectangular patches to cover the 4.85-GHz 5G MW band. The MMW microstrip array is fed by a coaxial probe at its center, and in the meanwhile the MMW array itself acts as the feed line of the MW patches, making the antenna structure compact. To isolate the MMW signal from the MW patches, a simple connection line is elaborately introduced between the MMW and MW elements. Therefore, using just a single port can obtain good radiation performance in both the MW and MMW bands, without requiring additional port or complicated filter. Owing to the simple structure, this antenna can be easily fabricated on a single-layer substrate using the traditional PCB technology. In addition, the operating frequencies of the MW band and MMW band can be adjusted independently, and a flexible frequency ratio ranging from 1.68 to >50 can be realized by using this antenna.

This manuscript is organized as follows. The configuration of the MW and MMW dual-band antenna is described in Section II, and the operating principle of the antenna is expatiated in Section III. In Section IV, the isolation and the flexible design of the two bands along with the range of the frequency ratio are discussed. An experimental verification is presented in Section V, and finally, a conclusion is drawn in Section VI.

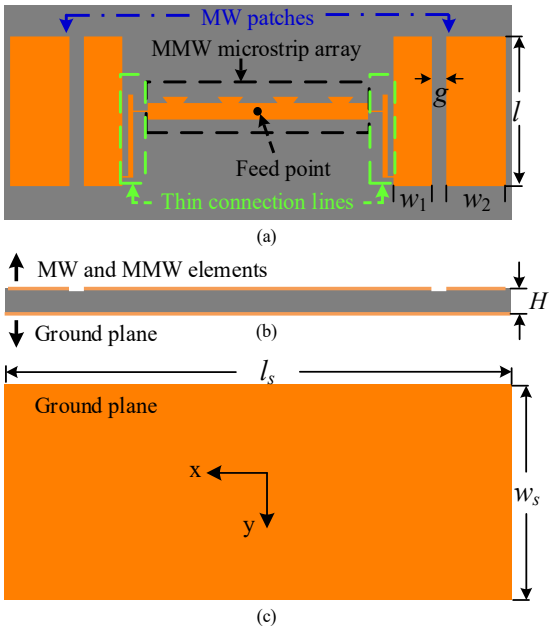

Fig. 1 Configuration of the proposed single-port dual-band antenna. (a) Top view. (b) Side view. (c) Bottom view. w_1 = 5.3 mm, w_2 = 8.2 mm, g = 2 mm, l = 20.1 mm, H = 0.787 mm, l_s = 70 mm, w_s = 29 mm.

II. Antenna Configuration

Fig. 1 shows the configuration of the proposed single-port dual-band antenna, which is designed on a single-layer dielectric substrate with a thickness of H = 0.787 mm and a relative permittivity of ε_r = 2.2. As shown in Fig. 1(a), this antenna is symmetric with respect to the y-axis at the central feed point, and it can be divided into three parts: 1) two identical slot-loaded rectangular patches, which are located at the left and right sides of the antenna, 2) a stub-loaded microstrip line, which is located in the middle of the antenna, and 3) two thin connection lines which connect the stub-loaded microstrip line and the slot-loaded rectangular patches. It will be shown in the following subsections that the two slot-loaded patches function as the radiating elements at MW band, while the stub-loaded microstrip line is able to radiate at MMW band effectively and simultaneously serve as the feeding network for the MW patch antenna. The two thin connection lines play an important role in guaranteeing the radiation performance of the antenna at the two bands. On one hand, they allow the MW signal to enter into the patches and excite in-phase currents on the two symmetrical patches. On the other hand, the thin connection lines also prevent the MMW signal from getting into the rectangular patches. A metal ground with length l_s = 70 mm and width w_s = 29 mm is used for the antenna, as shown in Fig. 1(c). In order to obtain broadside radiation patterns in the operating bands, a coaxial probe is applied to feed the dual-band antenna at the center, and the inner and outer conductors of the feeding probe are soldered to the microstrip line and the ground plane respectively. It can be seen that the entire antenna has a very simple configuration, which can be easily fabricated via the traditional PCB technology.

This antenna is designed to operate at 4.85 and 26 GHz bands concurrently for 5G wireless communication systems.

This article has been accepted for publication in a future issue of this journal, but has not been fully edited. Content may change prior to final publication. Citation information: DOI 10.1109/TVT.2021.3070807, IEEE Transactions on Vehicular Technology

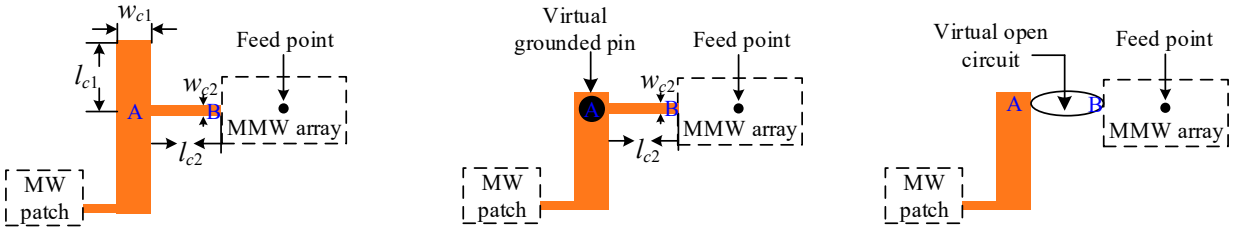

Fig. 2 (a) The connection lines between MW and MMW radiating elements. (b) Equivalent structure I. (c) Equivalent structure II. w_{c1} = 0.7 mm, l_{c1} = 2.25 mm, w_{c2} = 0.2 mm, l_{c2} = 2 mm.

III. Antenna Principle

In this section, the operating principle of the proposed antenna is expatiated.

A. The Isolation Between The MW And MMW Elements

As discussed in the Introduction, it is a big challenge to separately guide the MW and MMW signals to the corresponding radiators for a single-port dual-band antenna. In the previous designs, the CMRC filter [34] or the specific aperture coupling [35] had to be used, increasing the insertion loss and the complexity of the antenna unavoidably. In this work, a simple connection line is proposed to provide the isolation function, which does not destroy the antenna performance and can be fabricated easily on a single-layer substrate.

To demonstrate the isolation mechanism clearly, the configuration of the connection line is separately shown in Fig.2(a). It is notable that the MW and MMW radiators share the same feed port which is located at the center of the MMW element. As can be seen from Fig. 2(a), there is a 0.7-mm wide (w_{c1} = 0.7 mm) open stub, whose length l_{c1} = 2.25 mm is designed to be about 1/4 guide wavelength at the center frequency of MMW band. According to the transmission line theory, the voltage at point A becomes zero after travelling a distance of a quarter wavelength, and therefore, the open stub can be equivalent to or replaced by a shorting pin, as shown in Fig. 2(b). Owing to the virtual grounded pin, when the MMW signal reaches point A, the signal flows into the ground plane where the electric potential is zero. As a result, the MMW signal is truncated and prevented from transmitting to the MW rectangular patches.

With reference to Fig. 2(a) and Fig. 2(b), a thin line with width of w_{c2} = 0.2 mm is used between point A and the MMW element. The length of this thin line is designed to be l_{c2} = 2 mm, which is also close to 1/4 guide wavelength at the MMW frequency. Again, according to the transmission line theory, after travelling a distance of a quarter wavelength from the grounded point A, the current at point B becomes zero and point B can be considered as an open-circuited point. Therefore, Fig. 2(b) can be further equivalent to Fig. 2(c). It can be seen from Fig. 2(c) that the MW and MMW elements are not connected to each other at MMW band, and therefore, the isolation effect is achieved. However, when the antenna works at the MW band, the lengths of l_{c1} and l_{c2} are much less than 1/4 guide wavelength. Therefore, the above short-circuited and open-circuited effects disappear. Consequently, the MW signal can reach the patches through the connection lines.

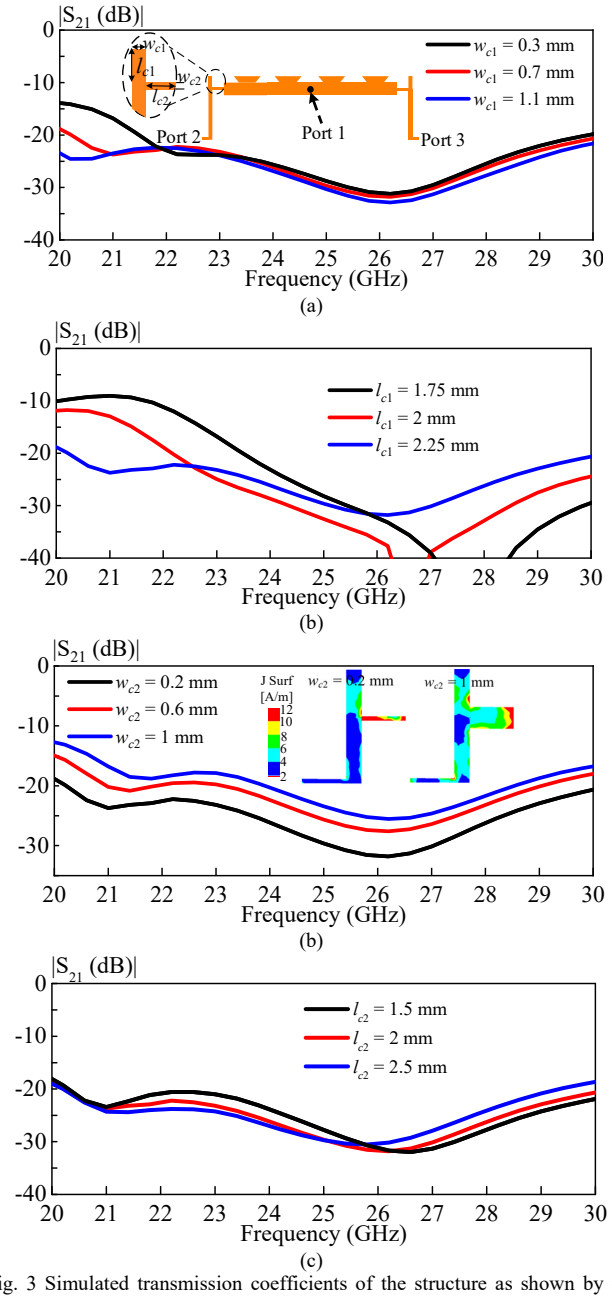

Fig. 3 Simulated transmission coefficients of the structure as shown by the inset in (a) for different parameters. (a) w_{c1}, (b) l_{c1}, (c) w_{c2}, and (d) l_{c2}.

This article has been accepted for publication in a future issue of this journal, but has not been fully edited. Content may change prior to final publication. Citation information: DOI 10.1109/TVT.2021.3070807, IEEE Transactions on Vehicular Technology

To quantify the effects of l_{c1}, w_{c1}, l_{c2} and w_{c2} on the isolation performance, the two MW patches in the dual-band antenna are replaced by two output ports, as shown in the inset of Fig. 3(a). Fig. 3 shows the simulated transmission coefficient $|S_{21}|$ (due to the structural symmetry, $|S_{31}|$ is the same with $|S_{21}|$ and therefore it is not shown for clarity) of the structure. It can be seen from Fig. 3(a) and (b) that the width of open stub w_{c1} has little effect on $|S_{21}|$ within the impedance passband, but the isolation frequency band with low $|S_{21}|$ shifts downward with the increasing of stub length l_{c1}. This is as expected, because as discussed above, the optimum isolation effect is achieved when l_{c1} is about 1/4 guide wavelength. On the other hand, the isolation level is found sensitive to the line width w_{c2}. With reference to Fig. 3(c), the $|S_{21}|$ is decreased by about 10 dB when w_{c2} is decreased from 1 to 0.2 mm, indicating that the thinner the line is, the better the isolation will be. This is because when w_{c2} is small, the current mainly distributes on the horizontal connection line, and very little current can cross the virtual grounded pin and flow into ports 2 and 3, as shown in the insets of Fig. 3(c). In addition, it is observed from Fig. 3(d) that the length of l_{c2} has negligible effect on $|S_{21}|$, but it affects the resonance frequency of the second mode in the MMW band. This is understandable, because only when l_{c2} equals to 1/4 guide wavelength of the working frequency of the MMW array, the virtual open-circuited effect appears at the ends of the MMW array and the MMW array is well isolated. Otherwise, the length of the central microstrip line will be increased or reduced by the horizontal connection line, and thus its resonance frequency is influenced.

To further verify the isolation mechanism discussed above, Fig. 4(a) and (b) show the current distributions of the dual-band antenna at MMW and MW bands, respectively. It can be seen from Fig. 4(a) that at the MMW frequency 26 GHz, the current mainly concentrates on the central stub-loaded microstrip line, and the currents on the connection lines and rectangular patches are negligibly weak, verifying the MMW signal can only feed the microstrip linear array but is isolated from the rectangular patches. The situation is quite different at the MW frequency 4.85 GHz. As shown in Fig. 4(b), the current distributes on the entire antenna structure. Specifically, it flows out from the feed point, goes through the MMW linear array and thin connection lines, and finally reaches the lateral rectangular patches, verifying the MW signal can feed the MW element perfectly. Moreover, it can be observed that in the MW band, the central stub-loaded microstrip line (MMW linear array) acts as the feed line of the MW patches. This is because at MW frequency the short stubs have very slight perturbation effect on the microstrip line due to the small electrical dimensions. Owing to the simple isolation mechanism and the shared structure, the entire antenna configuration is very compact.

B. The MMW Microstrip Array

As shown in Fig. 4(a), the MMW signal is restricted in the central stub-loaded microstrip line and prevented from flowing into the connection lines and rectangular patches, indicating that the stub-loaded microstrip line shown in Fig. 5(a) solely acts as the MMW radiating element and the remaining parts have trivial influence. Therefore, for simplicity, the separate stub-loaded microstrip array is utilized to illustrate the MMW performance of the proposed dual-band antenna. As shown in

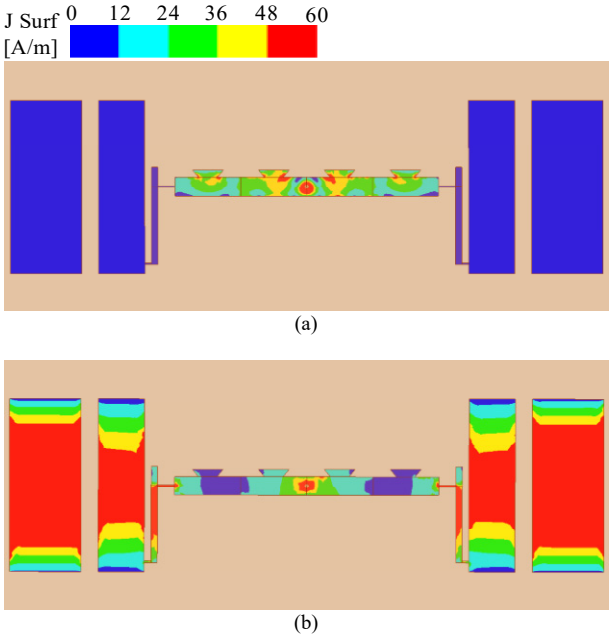

Fig. 4 The current distributions of the proposed single-port dual-band antenna at two operating bands. (a) 26 GHz and (b) 4.85 GHz.

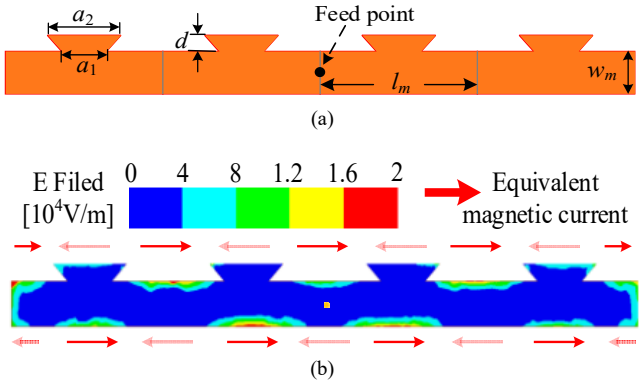

Fig. 5 (a) The MMW microstrip linear array. (b) The simulated electric field and equivalent magnetic current distributions on the microstrip array at 26 GHz. a_1 = 2.15 mm, a_2 = 3.55 mm, d = 0.84 mm, l_m = 7.6 mm, w_m = 2.2 mm.

Fig. 5(a), the microstrip array is composed of four identical radiating elements. Each element consists of a microstrip line with length l_m = 7.6 mm and width w_m = 2.2 mm, and a trapezoidal stub with top length a_1 = 2.15 mm, bottom length a_2 = 3.55 mm, and height d = 0.84 mm.

Since the stub-loaded microstrip array has been investigated in [37], the principle here is simply interpreted with Fig. 5(b), which shows the simulated E-field and also the equivalent magnetic current distributions on the sides of the microstrip array. It can be seen from Fig. 5(b) that due to the perturbation of the asymmetrically-introduced stubs, the fields on the two opposite long edges of the microstrip line become asymmetrical, and the intensities of the equivalent magnetic currents are unable to cancel each other out as in a pure microstrip line. Hence, the stub-loaded microstrip line is able to radiate effectively.

Fig. 6 shows the simulated reflection coefficient and boresight gain of the MMW microstrip linear array. Two

This article has been accepted for publication in a future issue of this journal, but has not been fully edited. Content may change prior to final publication. Citation information: DOI 10.1109/TVT.2021.3070807, IEEE Transactions on Vehicular Technology

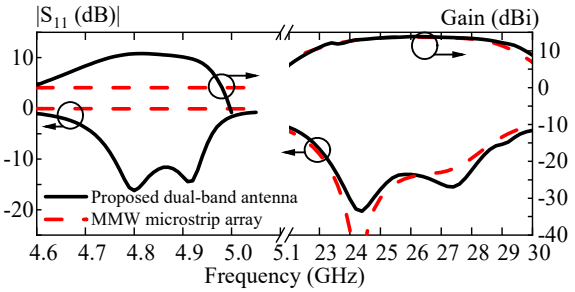

Fig. 6 Simulated reflection coefficients and gains of the single MMW microstrip linear array and the proposed single-port dual-band antenna.

resonant modes are excited in the MMW passband, at about 24.8 and 27.4 GHz respectively. It is found that the first mode is due to the resonance of the stub-loaded microstrip line, while the second one is caused by the resonance of the pure microstrip line [37]. The combination of the two modes helps engender an impedance bandwidth of about 20%. Within the impedance passsband, the antenna gain is quite stable, given by about 13.3 dBi. For comparison, the simulated reflection coefficient and boresight gain of the proposed dual-band antenna in Fig. 1 is also shown in Fig. 6. It is found that the response is very similar with that of the isolated microstrip linear array at MMW band. But in the MW band, the isolated MMW array has no operation while the proposed dual-band antenna operates well. These results verify again the analysis in Section IIIA.

C. The MW Microstrip Patches

As shown in Fig. 4(b), the entire structure of the proposed antenna is involved in the MW band. The stub-loaded microstrip line and the thin connection lines both act as the feed line, while the rectangular patches act as radiators. Since the feed line is symmetric with respect to the *y*-axis, the two patches are also placed symmetrically to have symmetric radiation patterns. As shown in Fig. 1, the length of the patches is given by $l = 20.1$ mm, which is about 1/2 guide wavelength at the MW band. It is found that the bandwidth of the rectangular patches is very limited owing to the thin substrate ($H = 0.787$ mm). In order to fully cover the frequency band 4.8–4.9 GHz, one of the 5G commercial MW band, a slot with width of $g = 2$ mm is introduced in each patch along the non-radiating edge. The slot divides the rectangular patch into two parts. The inner part with width of $w_1 = 5.3$ mm is fed directly by the thin connection line, while the outer part with width of $w_2 = 8.2$ mm is excited by the inner part through capacitive coupling.

To show the effect of the slot, Fig. 7 compares the simulated reflection coefficients of the proposed antenna at MW band for different slot widths. It can be seen that when there is no slot ($g = 0$ mm), only one resonant mode is excited at about 4.68 GHz, and the impedance bandwidth is as narrow as 1.5%. When introducing a 1-mm wide slot on the patch, two resonant modes are observed at 4.78 and 4.88 GHz. The two modes move close to each other when the slot width *g* is further increased to 2 mm, and good impedance matching is obtained in the band ranging from 4.77 to 4.95 GHz. Obviously, the introduction of slot greatly enhances the bandwidth of the MW band, making it sufficient for the 5G application.

In order to further characterize the two resonant modes in the MW operating band, Fig. 7(b) and (c) show the

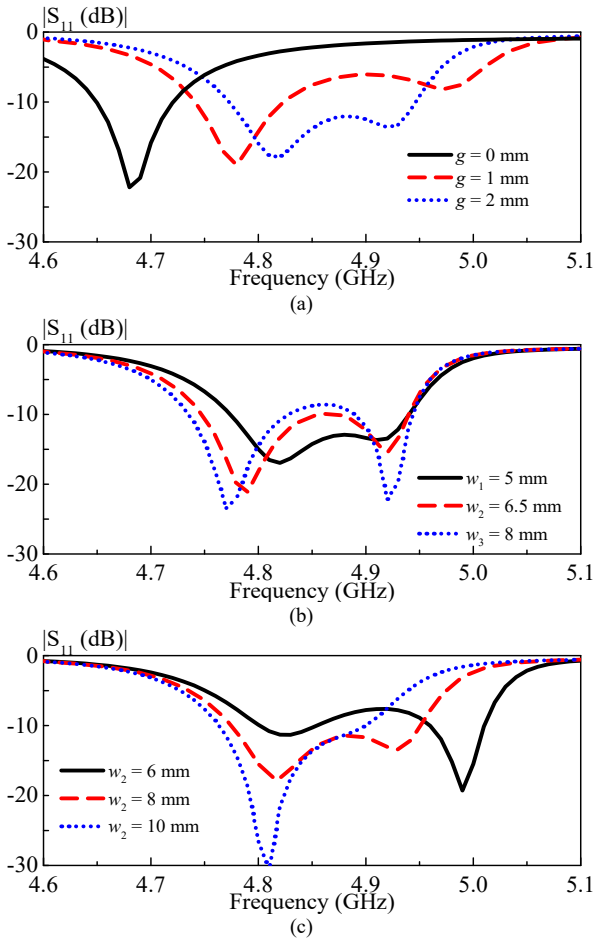

Fig. 7 Simulated reflection coefficients of the proposed single-port dual-band antenna at MW band, for different (a) slot widths *g*, (b) inner patch widths w_1, and (c) outer patch widths w_2.

simulated reflection coefficients of the proposed dual-band antenna for different widths of the inner patches (w_1) and outer patches (w_2), respectively. It can be observed that the first resonant mode shifts downward from 4.82 to 4.77 GHz when w_1 increases from 5 to 8 mm, but is insensitive to the variation of w_2. On the contrary, the second resonance frequency remains at about 4.92 GHz with the variation of w_1, but it shifts considerably from about 4.88 to 4.99 GHz when w_2 is decreased from 10 to 6 mm. These results indicate that the first resonant mode is due to the inner patch, while the second mode depends on the capacitively-coupled outer patch.

IV. Discussions

In this section, the influence of the isolation structure and the flexible design of the MW&MMW bands are further discussed.

A. The Influence of The Isolation Structure

As discussed in Section IIIA, the elaborately designed connection line plays an important role in reducing the interference between the MW and MMW bands. One potential question is that what would be the influence if not using such isolation structure. To answer this question, two reference antennas using different connections between the MW and MMW elements are investigated. Fig. 8 shows the

This article has been accepted for publication in a future issue of this journal, but has not been fully edited. Content may change prior to final publication. Citation information: DOI 10.1109/TVT.2021.3070807, IEEE Transactions on Vehicular Technology

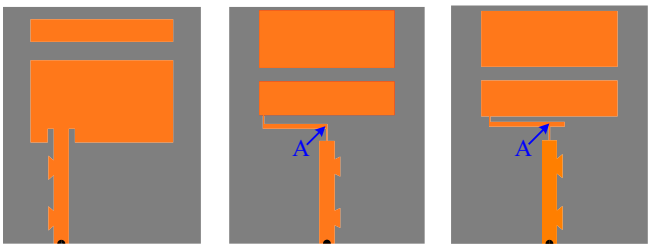

(a) (b) (c)

Fig. 8 Configurations of the reference and the proposed antennas. For simplicity, only half of the structure is shown due to the symmetry property. (a) Reference Antenna I. (b) Reference Antenna II. (c) The proposed antenna.

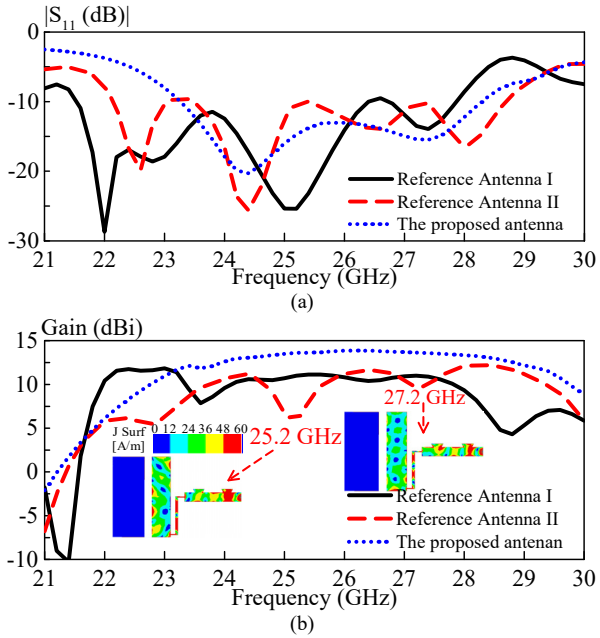

Fig. 9 Simulated reflection coefficients and boresight gains of the reference and the proposed antennas at MMW band. (a) Reflection coefficients. (b) Boresight gains, and the insets show the current distributions of reference Antenna II at 25.2 and 27.2 GHz.

configurations of the two reference antennas. For each antenna, only half of the structure is shown due to the symmetry property. In Antenna I, the MMW microstrip array is directly connected to the MW rectangular patches. Antenna II is very similar to the proposed antenna, except that the open stub at point A is removed from the connection line. It is notable that the dimensions of reference Antennas I and II have been re-optimized to adapt the change of the connection lines.

Fig. 9(a) shows the simulated reflection coefficients of the reference and the proposed antennas at MMW band (the antenna performances including the reflection coefficient, realized gain, and radiation pattern of the three antennas are nearly the same at MW band, therefore they are not shown here for brevity). It can be seen that the reflection coefficients vary greatly in the reference antennas although good impedance matching can also be obtained. Four resonant modes, instead of two, are excited in Antennas I and II within the operating band. This is because the connection ways between the MMW array and MW patches in both reference antennas have no isolation effect, and the MW patches also act as absorption or load elements of the MMW microstrip line. In this case, the patches have a great impact on the MMW array, leading to multiple modes at MMW band.

The simulated boresight gains of the reference and the proposed antennas at MMW band are compared in Fig. 9(b). It can be seen that the gains of Antennas I and II vary considerably (as large as 4 dB in Antenna I, and 6 dB in Antenna II) across the impedance passband. This is mainly because the currents on the patches destroy the radiation patterns at MMW band. Moreover, in Antenna I, to make the currents of the two symmetrical patch elements in-phase, the signal is fed at the side edge of the patches. Therefore, the MMW array of Antenna I is no longer in the center position with respect to the ground plane, and consequently, the maximum radiation in the E-plane (ϕ = 90°) deviates from the boresight direction to some extent. The MMW array of Antenna II is located at the center with respect to the ground plane, but the currents on the patches and connection lines still affect the radiation patterns. Particularly, at some frequency points like 25.2 and 27.2 GHz, the currents concentrate on the connection lines and inner MW patches as shown in the insets of Fig. 9(b), and the impedance matching is relatively poor, leading to a degraded gain. Differently, the boresight gain of the proposed antenna varies slightly from 11.98 to 13.87 dBi within the entire band, showing good stability. In addition, stable broadside patterns are obtained across the MMW passband.

Based on the above analysis, it can be concluded that the proposed connection lines are very necessary to maintain the stability of reflection coefficient, boresight gain and radiation pattern within the MMW band.

B. The Flexible Design of The MW&MMW Bands

For a dual-band antenna, it is very desirable that the two operating bands can be independently adjusted. As discussed in section IIIA, the patches are isolated from the microstrip array at MMW band, thus changing the parameters of patches should have no influence on the MMW band. At MW band, the microstrip array serves as the feed line for the patches, therefore the size adjustment of the microstrip line and trapezoidal stubs should have little effect on the working frequency of MW band. According to the analysis, the independent control of the lower MW band and the higher MMW band should be possible.

To verify the above inference, Fig. 10(a) shows the simulated reflection coefficients of the proposed antenna for different patch lengths of l = 19, 20, and 21 mm. It can be observed that in all of the three cases, the MMW operating band remains unchanged, keeping the center frequency at about 26 GHz. Nevertheless, the MW operating band changes substantially and its center frequency shifts downward significantly from 5.08 to 4.66 GHz when l increases from 19 to 21 mm. Accordingly, the frequency ratio is increased from 5.1 to 5.6. Fig. 10(b) shows the results for different lengths of the microstrip line l_m. It can be seen that the change of l_m only affects the impedance matching of the MW band but its center frequency remains at about 4.85 GHz. However, the higher MMW band is found sensitive to the variation of l_m. When l_m increases from 7.2 to 7.8 mm, the center frequency of MMW band increases from about 25 to 27 GHz, and the frequency ratio varies from 5.15 to 5.57.

As discussed above, the MMW microstrip linear array and the MW patch antenna can be independently designed and then

This article has been accepted for publication in a future issue of this journal, but has not been fully edited. Content may change prior to final publication. Citation information: DOI 10.1109/TVT.2021.3070807, IEEE Transactions on Vehicular Technology

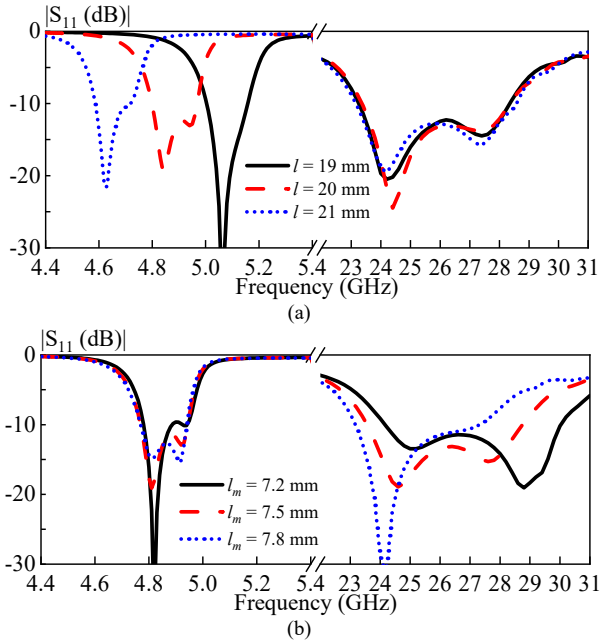

Fig. 10 Simulated reflection coefficients of the proposed single-port dual-band antenna for different (a) patch lengths l, and (b) microstrip-line lengths l_m.

cascaded with the specific connection lines. In general, if disregarding the low antenna efficiency, the operating frequency of the MMW array can be made extremely high while that of the MW patch can be made rather low. That is to say, theoretically, the upper bound of the obtainable frequency ratio can approach infinity. Even taking the efficiency into account, for example, if efficiency is required to be higher than 60%, the MW antenna can work down to 1 GHz when using the present substrate with thickness of 0.787 mm. Moreover, it is found that the simulated efficiency of the MMW array remains as high as 90% when it works at 50 GHz, showing that the maximum frequency ratio can be larger than 50. However, the lower bound of the frequency ratio is limited by the isolation effect of the connection lines. For illustration, we keep the working frequency of MMW array as well as the dielectric substrate of the present design unchanged, and determine the lower bound of the frequency ratio by identifying the possible highest operating frequency of the MW antenna. Here, it should be mentioned that as analyzed in Section IIIA, the dimensions of the open stub and the horizontal part of the connection lines are determined by the MMW operating band, therefore, they also remain unchanged. The structure as shown by the inset in Fig. 11 is used to quantify the isolation effect of the connection lines on the MW elements at different frequencies, and the corresponding results are shown in Fig. 11. It can be seen that in the frequency band that above 15.5 GHz, the signal is isolated by the connection lines and therefore the MW elements cannot be effectively excited. In the frequency band lower than 15.5 GHz, the $|S_{21}|$ varies with $|S_{11}|$ in the range of about −6.8 to −3.2 dB, and it is larger than −4 dB when $|S_{11}|$ is less than −10 dB. Notably, the structure of the inset in Fig. 11 has two output ports, and the maximum $|S_{21}|$ is −3 dB. The results indicate that the signal can be well guided to the MW elements only when the frequency is below 15.5 GHz. Based on the above analysis, the lower bound of the frequency ratio is given by about 1.68 (26/15.5). For validation, two design examples with different

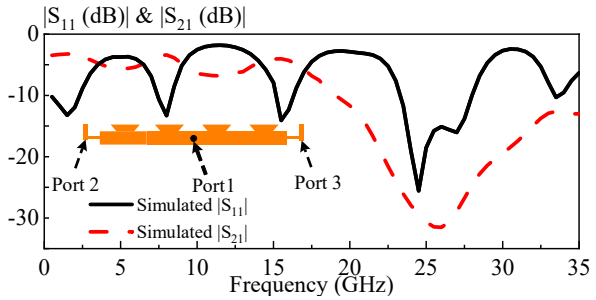

Fig. 11 Simulated reflection coefficient and transmission coefficient of the structure as shown by the inset.

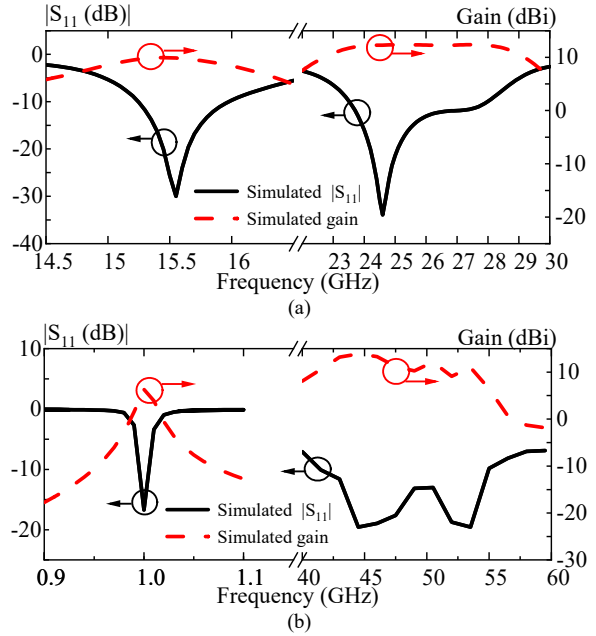

Fig. 12 Simulated reflection coefficients and boresight gains of the proposed antenna with different frequency ratios. (a) Design I with frequency ratio of 1.68 (26/15.5). (b) Design II with frequency ratio of 50 (50/1).

parameters are shown in Fig. 12. It can be seen from the figure that the frequency ratio of the proposed antenna can be tuned from 1.68 (26/15.5) to >50 (50/1).

It should be mentioned that the bounds of frequency ratio depend on the dielectric substrate to some extent, but the above analyses are still applicable.

In addition, since the variation of MW elements has little effect on the radiation performance of the MMW array as well as the isolation effect of the connection lines, the present MW patch can be re-designed or even replaced by a MW dual (multi)-band element to achieve a multi-frequency operation. For verification, the parameters of the MW patch elements of the proposed dual-band antenna are re-designed to realize the tri-band operation as shown in Fig. 13(a). Fig. 13(b) shows the simulated reflection coefficient and gain of the tri-band antenna. It can be seen that the antenna can simultaneously work at 4.85, 5.91 and 26 GHz (corresponding to 5G cellular networks, Vehicle-to-Vehicle, and 5G MMW bands), and the average boresight gains are given by 9.0, 7.0 and 12.4 dBi respectively.

All the above results are reasonable and as expected, showing well the design flexibility of the MW and MMW bands.

This article has been accepted for publication in a future issue of this journal, but has not been fully edited. Content may change prior to final publication. Citation information: DOI 10.1109/TVT.2021.3070807, IEEE Transactions on Vehicular Technology

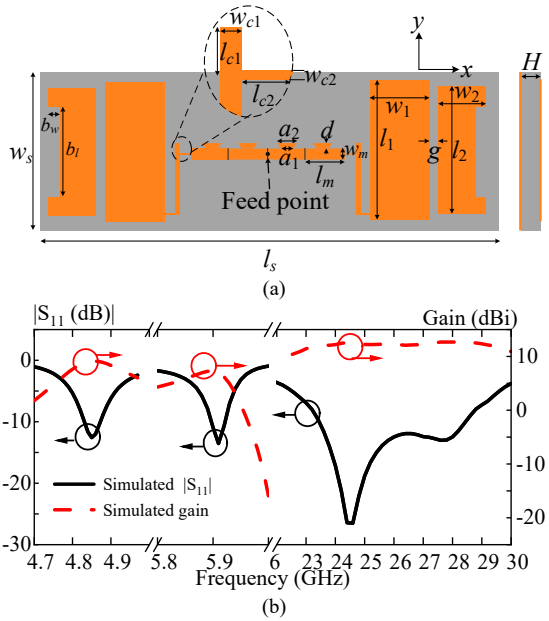

Fig. 13 (a) Configuration and (b) simulated reflection coefficients & boresight gains of the tri-band antenna. l_s = 80 mm, w_s = 25 mm, l_m = 7.6 mm, H= 0.787 mm, a_1 = 2.15 mm, a_2 = 3.55 mm, d = 0.84 mm, b_l = 12.6 mm, b_w = 2 mm, w_1 = 10.5 mm, w_2 = 8 mm, l_1 = 19.9 mm, l_2 = 15.7 mm , g = 0.2 mm, l_{c1} = 2.25 mm, w_{c1} = 0.7 mm, l_{c2} = 2 mm, w_{c2} = 0.2 mm.

V. Measurement Verification

For verification, a prototype of the proposed dual-band antenna operating at 4.85 and 26 GHz was fabricated and tested. Fig. 14 shows the top and bottom surfaces of the prototype which was fabricated by a PCB of Rogers RT/duroid 5880 with a thickness of 0.787 mm, a relative permittivity of 2.2, and a loss tangent of 0.0009. In this work, the reflection coefficient was measured by a Keysight N5247A PNA-X Network Analyzer, while the antenna gains and radiation patterns at 4.85-GHz band were tested using a Satimo Starlab System, and those at 26-GHz band were tested using a Compact Range Antenna Measurement System.

The measured and simulated refection coefficients of the prototype are shown in Fig. 15(a). It is notable that there are two resonant modes excited in both the 4.85-GHz MW band and 26-GHz MMW band. As discussed above, the first and the second modes in the MW band are due to the inner and outer rectangular patches respectively, while those in the MMW band are caused by the stub-loaded microstrip line and the bare microstrip line respectively. The dual-mode resonances enable the operating bands to completely cover the 5G commercial operating bands of 4.8−4.9 GHz and 24.75−27.5 GHz. As can be seen from the figure, the measured −10 dB impedance bandwidths at the MW and MMW bands are 3.10% (4.78−4.93 GHz) and 19% (23.81−28.81 GHz) respectively, agreeing reasonably well with the simulated results given by 3.70% (4.77−4.95 GHz) and 19.47% (23.27−28.29 GHz). The small deviation is mainly due to the simulation error, the fabrication error, and also the testing error [37].

Fig. 15(b) shows the simulated and measured boresight gains of the prototype, at the two operating bands. As shown in the figure, the peak and average simulated gains in the

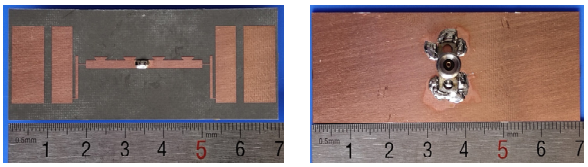

Fig. 14 Prototype of the proposed single-port dual-band antenna. (a) Top surface. (b) Bottom surface.

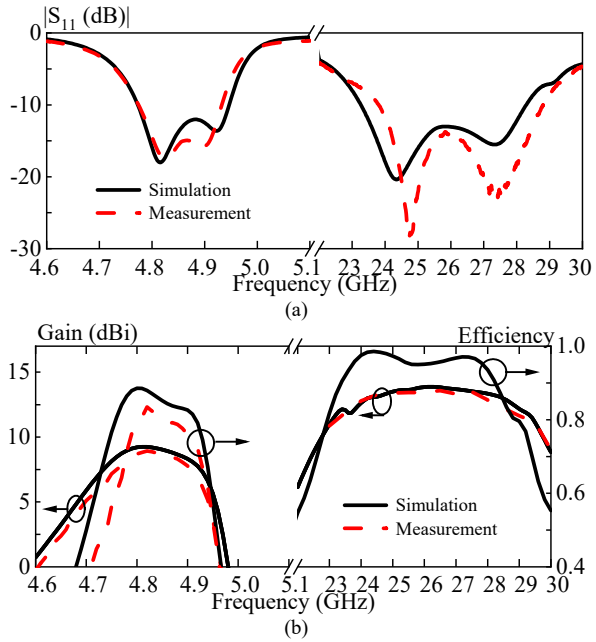

Fig. 15 Measured and simulated reflection coefficients, boresight gains, and efficiencies of the prototype. (a) Reflection coefficients. (b) Boresight gains and efficiencies.

4.85-GHz MW band are given by 9.25 and 8.45 dBi respectively, and those in the 26-GHz MMW band are 13.87 and 13.3 dBi respectively. The measured gains exhibit a very similar trend, but are generally about 0.3 dB lower than the simulated results at both bands. This is mainly caused by the imperfections of the experiment, such as the losses of the connecter and cable. In addition, it is notable that the gains in both the MW and MMW bands are fairly stable, and the measured 1-dB gain bandwidths are given by 2.28% and 16.7% respectively, which are very close to the −10 dB impedance bandwidths. The simulated and measured antenna efficiencies in the MW and MMW bands are also shown in Fig. 15(b). Notably, due to the limitation of the test conditions, the measured efficiency at the MMW band is not available. As shown in the figure, the simulated (measured) efficiency is about 0.85 (0.80) in the MW band, while as high as 0.95 in the MMW band. It should be mentioned that the relatively lower efficiency of the proposed antenna in the MW band is due to the thin dielectric substrate and has little to do with the connection lines.

Fig. 16 depicts the simulated and measured H-plane (ϕ = 0°) and E-plane (ϕ = 90°) radiation patterns at the two operating bands. In each band, the patterns at the two resonance frequencies are shown. With reference to Fig. 16(a), broadside radiation patterns are obtained in 4.85-GHz MW band. This is as expected considering the in-phase excitation of the two lateral patches. At the two resonance frequencies 4.83 and 4.9

This article has been accepted for publication in a future issue of this journal, but has not been fully edited. Content may change prior to final publication. Citation information: DOI 10.1109/TVT.2021.3070807, IEEE Transactions on Vehicular Technology

TABLE I
COMPARISON WITH THE PREVIOUS DUAL (MULTI)-BAND ANTENNAS WITH LARGER FREQUENCY RATIO

Ref.	Frequency (GHz)	Ratio	Impedance BW (%)	Peak gain (dBi)	Structure	Size (λ_L^3)	No. of input ports	Independent control of different bands
[25]	7.2/38.3	5.3	37.8/17	~16/~16	Two-layer SIW	–	4	yes
[26]	2.4/5.2/60	25	21.28/5.7/11.57	3.97/4.07/12.29	Single-layer SIW	1.29 × 0.36 × 0.008 @ 2.4 GHz	4	–
[27]	2.4/24	10	38.24/16.18	~7/11.3	3-D DRA	1.2 × 1.2 × 0.3	2	no
[29]	3.5/60	17	2.6/6.4	7.3/24	Multi-layer SIW	0.42 × 0.3 × 0.02	2	no
[31]	3.5/28	8	20.7/20.5	7.07/11.3	Single-layer SIW	0.5 × 0.4 × 0.003	2	no
[34]	4/60	15	85/13.3	4/7	Single-layer PCB	0.47 × 0.45 × 0.003	1	–
[35]	5.8/30	5.2	3.1/8.1	10.4/8.5	Two-layer SIW	1.64 × 1.64 × 0.02	1	yes
[36]	3.72/28.6	7.7	3.4/4.5	8.98/19.2	Differential-feed PCB	0.86 × 0.86 × 0.01	1	no
This work	4.85/26	5.4	3.1/19	8.93/13.57	Single-layer PCB	1.13 × 0.47× 0.013	1	yes

λ_L: vacuum wavelength at the center frequency of MW band
SIW: substrate-integrated waveguide.

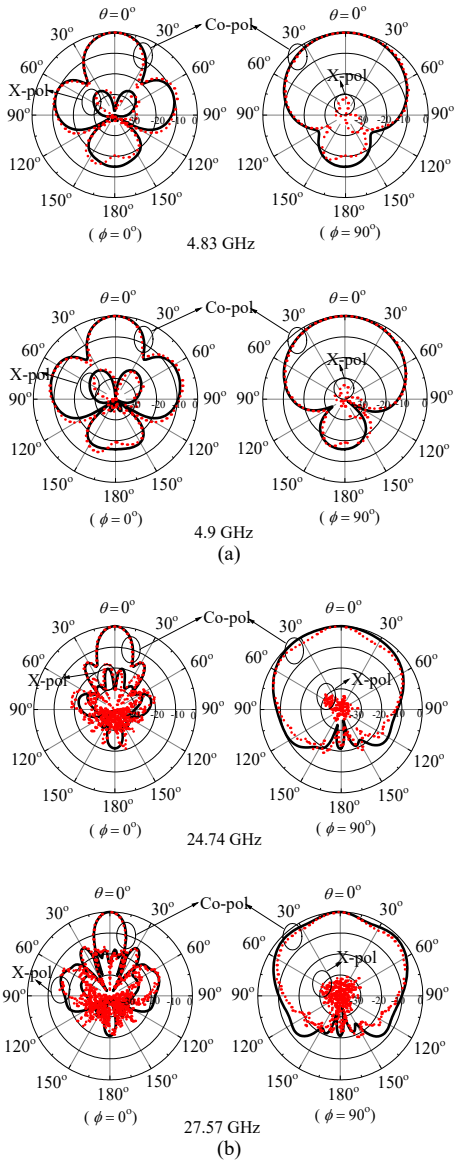

Fig. 16 Measured and simulated radiation patterns of the prototype. (a) At 4.83 and 4.9 GHz of the MW band. (b) At 24.74 and 27.57 GHz of the MMW band. ——— Simulated - - - - - - - Measured.

GHz, the E-plane patterns have a stable 3-dB beam-width of about 84°, while the 3-dB beam-widths of the H-plane patterns are about 36° and 32° respectively, and a sidelobe at about 68° can be observed. This is because the two rectangular patches are located symmetrically on the left and right sides of the antenna, and they can be regarded as a two-element array along the *x*-axis. The measured front-to-back ratios at the first and second resonance frequencies are both given by about 20 dB. In addition, the radiation patterns show a very low cross-polarization level in the boresight direction, and the measured cross-polarized fields are weaker than the co-polarized counterparts by more than 30 dB.

Broadside radiation patterns are also obtained in the 26-GHz MMW band, as shown in Fig. 16(b). At the two resonance frequencies 24.74 and 27.57 GHz, the radiation patterns are very similar. A narrow beam with a 3-dB beam-width of about 20° is measured in the H-plane, and a fan beam with a 3-dB beam-width of about 90° is obtained in the E-plane. In the boresight direction, the measured cross-polarization level and the front-to-back ratio are both given by about 20 dB.

A comprehensive comparison between the proposed antenna and the previously reported dual-band antennas with large frequency ratios is summarized in Table I. As shown in the table, most of the existing designs have two or four separate ports for MW band and MMW band respectively [25]–[27], [29], [31]. The dual-band antenna studied in [34] had a single port, but a complex low-pass CMRC filter was required to deal with the interference between the MW and MMW bands, which inevitably increased the design complexity and decreased the antenna gain as well as efficiency. The singly-fed dual-band antenna in [35] skillfully utilized a half-wavelength aperture to separate the MW and MMW signals, however, the coupling structure made the antenna suffer from a two-layer configuration. The singly-fed dual-band antenna was also realized in [36], nevertheless, a differential-feed network was required to improve the impedance matching, which complicated the design. The proposed antenna has a single port and a single-layer structure. Also, it does not need complicated filter and feeding network, making the structure simple and compact. In addition, it is notable that due to the shared structure, the two operating

bands of most of the previous antennas affect each other [27], [29], [31], [36]. Although the MMW band of [25] can be adjusted independently, the dielectric constant of the upper-layer substrate needs to be changed. However, the MW and MMW bands of the proposed antenna can be easily and independently adjusted by changing the corresponding parameters. Finally, it should be mentioned that compared with other designs, the footprint of the proposed antenna is slightly larger. This is because there are two radiating patch elements operating at the MW band and at the same time there are four microstrip elements operating at the MMW band. Owing to the above reason, the antenna gains at the two bands are also generally higher than those of others.

VI. Conclusion

This manuscript investigated a single-port, single-layer, dual-band antenna operating at 4.85-GHz MW and 26-GHz MMW 5G bands for wireless communication system. A stub-loaded microstrip line was adopted to cover the MMW band and simultaneously serve as the feed line of the rectangular patches operating at the MW band. Such structure-sharing topology makes the antenna structure fairly compact. Also, it has been shown that by using an elaborately-designed connection line to connect the MW patches and MMW array, the MW and MMW signals can be transmitted to the corresponding elements without affecting each other. No additional port or complicated filter is required, and the entire antenna has a simple configuration which can be easily fabricated on a single-layer substrate using the traditional PCB technology. Moreover, it has been found that the MW and MMW operating bands can be adjusted independently, and the frequency ratio can be tuned from 1.68 to >50.

A prototype has been fabricated and measured to verify the design. The prototype shows a −10-dB impedance bandwidth of 3.1% and a peak gain of 8.93 dBi at the 4.85-GHz MW band, while a −10-dB impedance bandwidth of 19% and a peak gain of 13.57 dBi at the 26-GHz MMW band.

The proposed dual-band antenna should have a potential application prospect in the 5G wireless communication systems.

Acknowkedgment

The valuable comments of the reviewers and editors are greatefully appreciated.

References

[1] S. Zhang, X. Chen and G. F. Pedersen, “Mutual Coupling Suppression With Decoupling Ground for Massive MIMO Antenna Arrays,” *IEEE Trans. Veh. Technol.*, vol. 68, no. 8, pp. 7273-7282, Aug. 2019.

[2] W. Hong, K. Baek, and S. Ko, “Millimeter-Wave 5G Antennas for Smartphones: Overview and Experimental Demonstration,” *IEEE Trans. Antennas Propag.*, vol. 65, no. 12, pp. 6250−6261, Dec. 2017.

[3] R. Rodriguez-Cano, K. Zhao, S. Zhang and G. F. Pedersen, “Handset Frame Blockage Reduction of 5G mm-Wave Phased Arrays Using Hard Surface Inspired Structure,” *IEEE Trans. Veh. Technol.*, vol. 69, no. 8, pp. 8132-8139, Aug. 2020.

[4] H. Ozpinar, S. Aksimsek and N. T. Tokan, “A Novel Compact, Broadband, High Gain Millimeter-Wave Antenna for 5G Beam Steering Applications,” *IEEE Trans. Veh. Technol.*, vol. 69, no. 3, pp. 2389-2397, March 2020.

[5] W. Hong et al., “Multibeam Antenna Technologies for 5G Wireless Communications,” *IEEE Trans. Antennas Propag.*, vol. 65, no. 12, pp. 6231−6249, Dec. 2017.

[6] C. Dehos, J. L. González, A. D. Domenico, D. Kténas and L. Dussopt, “Millimeter-Wave Access and Backhauling: The Solution to the Exponential Data Traffic Increase in 5G Mobile Communications Systems?” *IEEE, Commun. Mag.*, vol. 52, no. 9, pp. 88−95, September 2014.

[7] M. M. Samadi Taheri, A. Abdipour, S. Zhang and G. F. Pedersen, “Integrated Millimeter-Wave Wideband End-Fire 5G Beam Steerable Array and Low-Frequency 4G LTE Antenna in Mobile Terminals,” *IEEE Trans. Veh. Technol.*, vol. 68, no. 4, pp. 4042-4046, April 2019.

[8] A. Pfadler, C. Ballesteros, J. Romeu and L. Jofre, “Hybrid Massive MIMO for Urban V2I: Sub-6 GHz vs mmWave Performance Assessment,” *IEEE Trans. Veh. Technol.*, vol. 69, no. 5, pp. 4652-4662, May 2020.

[9] H. Zhou, W. Xu, J. Chen and W. Wang, “Evolutionary V2X Technologies Toward the Internet of Vehicles: Challenges and Opportunities,” *Proceedings of the IEEE*, vol. 108, no. 2, pp. 308-323, Feb. 2020.

[10] J. Lianghai, A. Weinand, B. Han and H. D. Schotten, “Applying Multiradio Access Technologies for Reliability Enhancement in Vehicle-to-Everything Communication,” *IEEE Access*, vol. 6, pp. 23079-23094, 2018.

[11] Y. Liu, X. Li, L. Yang and Y. Liu, “A Dual-Polarized Dual-Band Antenna With Omni-Directional Radiation Patterns,” *IEEE Trans. on Antennas Propag.*, vol. 65, no. 8, pp. 4259−4262, Aug. 2017.

[12] D. Wu, S. W. Cheung and T. I. Yuk, “A Compact and Low-Profile Loop Antenna With Multiband Operation for Ultra-Thin Smartphones,” *IEEE Trans. on Antennas Propag.*, vol. 63, no. 6, pp. 2745−2750, June 2015.

[13] X. Dai, T. Zhou and G. Cui, “Dual-Band Microstrip Circular Patch Antenna With Monopolar Radiation Pattern,” *IEEE Antennas Wireless Propag. Lett.*, vol. 15, pp. 1004−1007, 2016.

[14] T. Yue, Z. H. Jiang and D. H. Werner, “A Compact Metasurface-Enabled Dual-Band Dual-Circularly Polarized Antenna Loaded With Complementary Split Ring Resonators,” *IEEE Trans. on Antennas Propag.*, vol. 67, no. 2, pp. 794−803, Feb. 2019.

[15] J. Ou, A. S. Andrenko, Y. Li, Q. Zhang and H. Tan, “High-Efficiency and Wide-Frequency-Ratio Dual-Band Slot Patch Antenna Utilizing the Perturbed TM02 Modes,” *IEEE Antennas Wireless Propag. Lett.*, vol. 17, no. 4, pp. 579−582, April 2018.

[16] Q. Wu, J. Yin, C. Yu, H. Wang and W. Hong, “Low-Profile Millimeter-Wave SIW Cavity-Backed Dual-Band Circularly Polarized Antenna,” *IEEE Antennas Wireless Propag. Lett.*, vol. 65, no. 12, pp. 7310−7315, Dec. 2017.

[17] P. Liu, X. Zhu, Y. Zhang, X. Wang, C. Yang and Z. H. Jiang, “Patch Antenna Loaded With Paired Shorting Pins and H-Shaped Slot for 28/38 GHz Dual-Band MIMO Applications,” *IEEE Access*, vol. 8, pp. 23705−23712, 2020.

[18] L. Zhang, K. Y. See, B. Zhang and Y. P. Zhang, “Integration of Dual-Band Monopole and Microstrip Grid Array for Single-Chip Tri-Band Application,” *IEEE Trans. on Antennas Propag.*, vol. 61, no. 1, pp. 439−443, Jan. 2013.

[19] Z. H. Tu, Y. P. Zhang, C. Luxey, A. Bisognin, D. Titz and F. Ferrero, “A Ceramic Antenna for Tri-Band Radio Devices,” *IEEE Trans. on Antennas Propag.*, vol. 61, no. 11, pp. 5776−5780, Nov. 2013.

[20] J. Qian, M. Tang, Q. Chen, Y. Zhang and J. Mao, “Integration of S/Ka/D-Band Antennas in LTCC With a Cylindrical Radome for Triband Applications,” *IEEE Trans. on Antennas Propag.*, vol. 67, no. 9, pp. 5781−5789, Sept. 2019.

[21] Y. Sun and K. W. Leung, “Substrate-Integrated Two-Port Dual-Frequency Antenna,” *IEEE Trans. on Antennas Propag*., vol. 64, no. 8, pp. 3692−3697, Aug. 2016.

[22] W. Menzel, M. Al-Tikriti and M. B. Espadas Lopez, “Common Aperture, Dual Frequency Printed Antenna (900 MHz and 60 GHz),” *Electron. Lett.*, vol. 37, no. 17, pp. 1059−1060, 16 Aug. 2001.

[23] T. Li and Z. N. Chen, “Shared-Surface Dual-Band Antenna for 5G Applications,” *IEEE Trans. on Antennas Propag.*, vol. 68, no. 2, pp. 1128−1133, Feb. 2020.

[24] C. Han, C. Rodenbeck, J. Huang and Kai Chang, “A C/ka Dual Frequency Dual Layer Circularly Polarized Reflectarray Antenna With Microstrip Ring Elements,” *IEEE Trans. on Antennas Propag*, vol. 52, no. 11, pp. 2871−2876, Nov. 2004.

[25] Y. Li and J. Wang, “Dual-Band Leaky-Wave Antenna Based on Dual-Mode Composite Microstrip Line for Microwave and Millimeter-Wave

Applications," *IEEE Trans. on Antennas Propag.*, vol. 66, no. 4, pp. 1660−1668, April 2018.
[26] Y. R. Ding and Y. J. Cheng, "A Tri-Band Shared-Aperture Antenna for 2.4/5.2 GHz Wi-Fi Application With MIMO Function and 60 GHz Wi-Gig Application With Beam-Scanning Function," *IEEE Trans. on Antennas Propag.*, vol. 68, no. 3, pp. 1973−1981, March 2020.
[27] L. Y. Feng and K. W. Leung, "Wideband Dual-Frequency Antenna With Large Frequency Ratio," *IEEE Trans. on Antennas Propag*, vol. 67, no. 3, pp. 1981−1986, March 2019.
[28] L. Y. Feng and K. W. Leung, "Dual-Fed Hollow Dielectric Antenna for Dual-Frequency Operation With Large Frequency Ratio," *IEEE Trans. on Antennas Propag.*, vol. 65, no. 6, pp. 3308−3313, June 2017.
[29] J. F. Zhang, Y. J. Cheng, Y. R. Ding and C. X. Bai, "A Dual-Band Shared-Aperture Antenna With Large Frequency Ratio, High Aperture Reuse Efficiency, and High Channel Isolation," *IEEE Trans. on Antennas Propag.*, vol. 67, no. 2, pp. 853−860, Feb. 2019.
[30] J. Chen, S. Cao and X. Zhang, "SPPs-Shared Dual-Band Antenna With Large Frequency Ratio," *IEEE Access*, vol. 8, pp. 29132−29139, 2020.
[31] J. Lan, Z. Yu, J. Zhou and W. Hong, "An Aperture-Sharing Array for 3.5/28 GHz Terminals with Steerable Beam in Millimeter Wave Band," *IEEE Trans. on Antennas Propag.*, vol. 68, no. 5, pp. 4114−4119, May 2020.
[32] Y. R. Ding and Y. J. Cheng, "Ku/Ka Dual-Band Dual-Polarized Shared-Aperture Beam-Scanning Antenna Array With High Isolation," *IEEE Trans. on Antennas Propag.*, vol. 67, no. 4, pp. 2413−2422, April 2019.
[33] M. Ikram, N. Nguyen-Trong and A. Abbosh, "Multiband MIMO Microwave and Millimeter Antenna System Employing Dual-Function Tapered Slot Structure," *IEEE Trans. on Antennas Propag.*, vol. 67, no. 8, pp. 5705−5710, Aug. 2019.
[34] D. Wang and C. H. Chan, "Multiband Antenna for WiFi and WiGig Communications," *IEEE Antennas Wireless Propag. Lett.*, vol. 15, pp. 309−312, 2016.
[35] B. J. Xiang, S. Y. Zheng, H. Wong, Y. M. Pan, K. X. Wang and M. H. Xia, "A Flexible Dual-Band Antenna With Large Frequency Ratio and Different Radiation Properties Over the Two Bands," *IEEE Trans. on Antennas Propag.*, vol. 66, no. 2, pp. 657−667, Feb. 2018.
[36] G. Xu, H. Peng, Z. Shao, L. Zhou, Y. Zhang and W. Yin, "Dual-Band Differential Shifted-Feed Microstrip Grid Array Antenna With Two Parasitic Patches," *IEEE Trans. on Antennas Propag.*, vol. 68, no. 3, pp. 2434−2439, March 2020.
[37] Y. Q. Guo, Y. M. Pan, and S. Y. Zheng, "Design of Series-Fed, Single-Layer, and Wideband Millimeter Wave Microstrip Arrays," *IEEE Trans. on Antennas Propag.*, vol. 68, no. 10, pp. 7017-7026, Oct. 2020.

Yu Qing Guo was born in Jiangxi Province, China. She is currently pursuing the M.Eng. degree with the School of Electronic and Information Engineering, South China University of Technology, Guangzhou, China. Her current research interests include millimeter wave microstrip antennas and dual-band antennas.

Yong Mei Pan (M'11–SM'17) was born in Huangshan, Anhui Province, China. She received the B.Sc. and Ph.D. degrees in electrical engineering from the University of Science and Technology of China, Hefei, China, in 2004 and 2009, respectively. From 2009 to 2012, she was a Research Fellow with the Department of Electronic Engineering, City University of Hong Kong, Kowloon Tong, Hong Kong. In 2013, she joined the School of Electronic and Information Engineering, South China University of Technology (SCUT), Guangzhou, China, as an Associate Professor. Currently, she is a Professor with SCUT. Her research interests include dielectric resonator antennas, leaky wave antennas, metasurface antennas, and filtering antennas.

Prof. Pan is now an Associate Editor of the IEEE Transactions on Antennas and Propagation.

Shao Yong Zheng (S'07-M'11-SM'17) was born in Fujian Province, China. He received the B.S. degree in electronic engineering from Xiamen University, Fujian, China, in 2003, the M.Sc., M. Phil and Ph. D degree in electronic engineering from City University of Hong Kong, Kowloon, Hong Kong, in 2006, 2008, and 2011 respectively.

From 2011 to 2012, he was a Research Fellow with Department of Electronic Engineering, City University of Hong Kong. He was a Visiting Assistant Professor with Department of Electronic Engineering, City University of Hong Kong from July 2013 to August 2013, from July 2014 to August 2014 and from Jul. 2015 to Aug. 2015. He is currently a Full Professor with School of Electronics and Information Technology, Sun Yat-sen University, Guangzhou, China, and the deputy director of Mobile Communication National Engineering Research Center, SYSU Branch. His research interests include microwave/millimeter wave components and evolutionary algorithms.

Dr. Zheng has published over 100 internationally refereed journal and conference papers including 60 IEEE Transactions papers. He has served as a Technical Program Committee Member and Session Organizer/Chair for a number of conferences (ICUWB, ACES, APCAP, iWEM, etc.). He is now an Associate Editor of the IEEE Antennas and Wireless Propagation Letters and Microwave and Optical Technology Letters.

Kai Lu was born in Hebei Province, China. He received the B.Eng. and M.Eng. degrees from Harbin Institute of Technology, Harbin, China, in 2006 and 2008, respectively, and the Ph.D. degree in 2012 from City University of Hong Kong (CityU), Hong Kong, all in electronic engineering.

He was a Post-Doctoral Fellow with CityU from 2012 to 2014. After that, he continued his research as a Visiting Scholar with Syracuse University, NY, USA, for one year. From 2016 and 2019, he was a Senior Antenna Engineer with Antenna Company, Eindhoven, The Netherlands. In 2020, he joined Sun Yat-sen University, Guangzhou, China, where he is currently an Associate Professor. His research interests include Fabry–Perot resonator antennas, dielectric resonator antennas, reflector antennas, horn antennas, microstrip patch antennas, metal-stamped antennas, 3-D-printed antennas, MIMO antennas, antenna arrays, millimeter wave imaging, reconstruction of antenna radiation pattern, and microwave theory.